Photon-absorption-induced intersubband optical-phonon scattering of electrons in quantum wells

T. Apostolova, Danhong Huang, and D. A. Cardimona
Air Force Research Lab, Space Vehicles Directorate, Kirtland Air Force Base, New Mexico 87117
(Received 9 August 2002; revised manuscript received 6 December 2002; published 28 May 2003)

In the presence of a normally incident intense mid-IR pulsed laser field, both photon-absorption-induced intrasubband and intersubband phonon-scattering of electrons are found by including the photon-assisted phonon-scattering process in a Boltzmann equation for phonon energies that are smaller than the energy separation between two electron subbands in a quantum well. The ultrafast dynamics of the electron distributions for different subbands is studied with various lattice temperatures, photon energies, field strengths, and quantum-well widths. Upward steps found in the differences between the electron distributions with/without the photon-assisted process are attributed to either photon-absorption-induced phonon scattering of electrons via intrasubband transitions or the photon-absorption-induced phonon scattering of electrons via intersubband transitions in quantum wells. The photon-absorption-induced phonon absorption by intersubband transitions of electrons from the first to the second subband is a unique feature in quantum-well systems and is found to have a significant effect on the electron populations in both subbands.

DOI: 10.1103/PhysRevB.67.205323 PACS number(s): 73.21.Fg, 61.80.Az, 61.80.Ba, 61.82.Fk

I. INTRODUCTION

Our understanding of steady-state transport properties of electron gases is primarily based on either the Kubo linear-response quantum theory or simply the Boltzmann transport equations.[1] It has been of great interest to extend these theories to situations beyond the weak-field perturbation regime.[2] The most useful description has been the semiclassical theory for electron dynamics supplemented by the Boltzmann equations for quantum statistics.[3] A more rigorous quantum-statistical theory[4] has revealed that the transport of electrons coupled to a strong electromagnetic field is only determined by the center-of-mass motion through a force balance (Newton-like) equation. However, the quantum-friction force in this force balance equation depends on the relative scattering motion of drifting electrons with static impurity atoms or vibrational lattices.[5] The simplest description of this electron relative scattering motion is the use of Boltzmann equations[6] in steady state although the density-matrix equations[7] have been widely employed to study the ultrafast dynamics of electrons weakly coupled to an external electromagnetic field. The so-called phonon-assisted ''optical transition'' of electrons under a nonresonant intense electromagnetic field is proved to be directly related to the field-induced center-of-mass acceleration, instead of single-electron transitions,[8] and not well understood,[2] e.g., the connection to the Joule heating and field-dependent diffusion and antidiffusion.[9] One must go beyond the perturbation limit to describe adequately the ultrafast dynamics of electrons in transient state. In addition, to describe the ultrafast dynamics of quantized electrons in multisubband quantum wells, one must generalize the single-band Boltzmann equations.[2]

Phonon scattering of electrons is an inelastic process and is associated with hot-electron energy dissipation. It causes electron mobility to decrease with increasing temperature, which greatly affects the electron transport through quantum-well systems,[1,10] and it also broadens both absorption and photoluminescence peaks, which alters the optical response of electrons in quantum wells.[11] Moreover, phonon-mediated nonradiative (Auger) electron-hole recombination at room temperature defines a threshold current density beyond which lasing in quantum wells can happen.[12] Besides these drawbacks, hot electrons injected from the contact layer can benefit from fast energy relaxation due to phonon emission to the band edge[13] before they radiatively recombine with injected holes in bipolar semiconductor laser devices. In a study of laser damage to bulk dielectric materials, phonon-assisted intraband photon absorption by conduction electrons[2] under a normally incident, intense, near-IR laser field was found to be the main energy-gain mechanism required for impact ionization.

For pulsed laser fields, a quantum density-matrix equation with collision integrals is widely used for calculations of steady-state or time-resolved optical spectra,[7] where the photon-induced coherence (nonzero off-diagonal density-matrix elements) plays a major role. The pulsed laser field in the current study does not directly couple to intersubband electron transitions due to the plane-polarized field and small photon energy compared to the energy separation between the two lowest subbands. Its role is limited to thermal heating of electrons with assistance from phonon scattering. Within this limit, the Boltzmann equation,[2,14] even the Fokker-Planck equation[9] under approximation, is found to be adequate for the calculation of hot-electron distributions.

In this paper, in the presence of a normally incident, intense, mid-IR pulsed laser field, the unique photon-absorption-induced optical-phonon absorption by electrons undergoing intersubband transitions from the first to the second subband in quantum wells is discovered by including photon-assisted phonon-scattering processes in a Boltzmann equation beyond the relaxation-time approximation[15] for phonon energies smaller than the energy separation between two subbands. We calculate the difference between the electron distributions with/without the photon-assisted phonon-scattering process in two subbands for various lattice temperatures, photon energies, laser field strengths, and

quantum-well widths. The effect of the photon-absorption-induced phonon-scattering by intersubband electron transitions on electron populations in the two lowest quantum-well subbands is evaluated.

The organization of the paper is as follows. In Sec. II, we introduce a photon-assisted optical-phonon-scattering model in quantum-well systems. Numerical results and discussions are given in Sec. III for the photon-absorption-induced intersubband phonon scattering of electrons. The paper is briefly concluded in Sec. IV.

II. MODEL AND THEORY

Let us consider a uniformly doped quantum well with electron confinement in the z (growth) direction. For a uniform electromagnetic field polarized in the quantum-well plane perpendicular to z, we assume a vector potential $\mathbf{A}(t)=[\mathcal{A}(t),0,0]$ as a result of rotational invariance of the system in the plane. By using the Coulomb gauge $\boldsymbol{\nabla}\cdot\mathbf{A}=0$, the single-particle Hamiltonian for the system in the presence of vector potential $\mathbf{A}$ is given by

$$\mathcal{H}_0=-\frac{\hbar^2}{2m^*}\frac{\partial^2}{\partial x^2}-\frac{ie\hbar}{m^*}\mathcal{A}(t)\frac{\partial}{\partial x}+\frac{e^2\mathcal{A}^2(t)}{2m^*}-\frac{\hbar^2}{2m^*}\frac{\partial^2}{\partial y^2}-\frac{\hbar^2}{2m^*}\frac{\partial^2}{\partial z^2}+U_{\mathrm{QW}}(z), \tag{1}$$

where m^* is the effective mass of electrons and $U_{\mathrm{QW}}(z)$ represents the quantum-well potential profile. For the Hamiltonian in Eq. (1), using the time-dependent Schrödinger equation we get the total wave function for conduction electrons[16]

$$\Psi_{n,k_x,k_y}(\mathbf{r}_\parallel,z;t)=\frac{1}{\sqrt{\mathcal{S}}}\exp(i\mathbf{k}_\parallel\cdot\mathbf{r}_\parallel)\phi_n(z)\exp\{-(i/\hbar)[E_n(k_\parallel)+2\gamma\hbar\Omega_{\mathrm{L}}]t\}\exp[i\gamma\sin(2\Omega_{\mathrm{L}}t)]\times\exp\{ik_xR_0[1-\cos(\Omega_{\mathrm{L}}t)]\}, \tag{2}$$

where we have assumed that $\mathcal{A}(t)=\mathcal{A}_0\sin(\Omega_{\mathrm{L}}t)\,\theta(t)$ with $\theta(t)$ being a step function. Here, $\mathcal{S}$ is the sample cross-sectional area, $\mathbf{r}_\parallel=(x,y)$, and $\mathbf{k}_\parallel=(k_x,k_y)$ are the two-dimensional position and wave vectors in the quantum-well plane, $n=1,2,3,\ldots$ is the index of the quantum-well subbands due to quantum confinement in the z direction, $R_0=e\mathcal{E}_0/m^*\Omega_{\mathrm{L}}^2$, and $\gamma=e^2\mathcal{E}_0^2/8m^*\hbar\Omega_{\mathrm{L}}^3$ with $\mathcal{E}_0=-\Omega_{\mathrm{L}}\mathcal{A}_0$. In Eq. (2), the quantum-well wave function $\phi_n(z)$ is determined from

$$\left[-\frac{\hbar^2}{2m^*}\frac{\partial^2}{\partial z^2}+U_{\mathrm{QW}}(z)\right]\phi_n(z)=E_n^z\phi_n(z), \tag{3}$$

where E_n^z is the edge of the nth subband in the quantum well. Moreover, the electron kinetic energy $E_n(k_\parallel)$ introduced in Eq. (2) is given by $E_n(k_\parallel)=E_{k_\parallel}+E_n^z$, with $E_{k_\parallel}=\hbar^2k_\parallel^2/2m^*$ due to free motion of electrons within the quantum-well plane.

In this paper, we only consider the scattering of electrons with optical phonons, since it is believed to be the most significant for polar semiconductors at room temperature. By using Eq. (2) and first-order time-dependent perturbation theory, the transition rate between initial and final electron states, Ψ_{n,k_x,k_y} and $\Psi_{n',k_x',k_y'}$, is found to be[17]

$$\mathcal{W}_{n,k_x,k_y;\to n',k_x',k_y'}=\frac{2\pi\alpha}{\hbar\mathcal{S}}\sum_{\mathbf{q}_\parallel}\delta_{\mathbf{k}_\parallel',\mathbf{k}_\parallel-\mathbf{q}_\parallel}\mathcal{F}_{nn'}(q_\parallel)\sum_{M=-\infty}^{+\infty}J_{|M|}^2(|q_xR_0|)\times\delta[E_{n'}(k_\parallel')-E_n(k_\parallel)-M\hbar\Omega_{\mathrm{L}}\pm\hbar\omega_{\mathrm{LO}}]. \tag{4}$$

Here, ω_{LO} is the frequency of longitudinal-optical phonons, $\mathbf{q}=(\mathbf{q}_\parallel,q_z)$ is the wave vector of phonons with $\mathbf{q}_\parallel=(q_x,q_y)$, $\alpha=(e^2/2\epsilon_0)\hbar\omega_{\mathrm{LO}}[1/\epsilon_{\mathrm{r}}(\infty)-1/\epsilon_{\mathrm{r}}(0)]$ is the electron-phonon coupling constant with $\epsilon_{\mathrm{r}}(\infty)$ and $\epsilon_{\mathrm{r}}(0)$ being the relative optical and static dielectric constants, respectively, the $\pm$ signs stand for phonon emission and absorption, $J_M(x)$ is the Mth-order Bessel function, and the Coulomb-interaction form factor $\mathcal{F}_{nn'}(q_\parallel)$ is given by

$$\mathcal{F}_{nn'}(q_\parallel)=\frac{1}{2(q_\parallel+q_{\mathrm{TF}})}\int_{-\infty}^{+\infty}dz\int_{-\infty}^{+\infty}dz'\,\phi_n^*(z)\times\phi_{n'}^*(z')e^{-q_\parallel|z-z'|}\phi_n(z')\phi_{n'}(z), \tag{5}$$

where $q_{\mathrm{TF}}=[e^2/2\pi\epsilon_0\epsilon_{\mathrm{r}}(0)](m^*/\pi\hbar^2)$ is the inverse of the Thomas-Fermi screening length.

It is well known that intrasubband electron transitions cannot directly respond to a uniform laser field due to violation of momentum conservation. However, we find from Eq. (4) that with the help of phonon-scattering, incident photons can be absorbed by intrasubband ($n=n'$) electron transitions. This type of phonon-assisted photon absorption ($M\neq0$) has also been called phonon-assisted free-carrier absorption.[2] Moreover, the intersubband electron transitions cannot directly respond to a plane-polarized laser field through dipole coupling due to selection rules. Although we find from Eq. (4) that the intersubband optical-phonon-scattering of electrons ($n\neq n'$) is prohibited for $M=0$, where $\hbar\omega_{\mathrm{LO}}<|E_{n'}(|\mathbf{k}_\parallel\pm\mathbf{q}_\parallel|)-E_n(k_\parallel)|$, the photon-assisted intersubband optical-phonon-scattering with $M\neq0$ becomes possible due to renormalization of the electron-phonon interaction in the quantum well by a laser field.

For a given electron state Ψ_{n,k_x,k_y}, from the calculated transition rate in Eq. (4) we obtain the total scattering-in rate $\mathcal{W}_{n,\mathbf{k}_\parallel}^{(\mathrm{in})}$ and scattering-out rate $\mathcal{W}_{n,\mathbf{k}_\parallel}^{(\mathrm{out})}$, from which we arrive at the following Boltzmann equation[9] for the electron distribution $f_n(E_n^z+E_{k_\parallel},t)$ in each subband

$$\frac{\partial}{\partial t}f_n(E_n^z+E_{k_\parallel},t)=\frac{2\pi\alpha}{\hbar\mathcal{S}}[1-f_n(E_n^z+E_{k_\parallel},t)]\sum_{n',\mathbf{q}_\parallel}\mathcal{F}_{nn'}(q_\parallel)\sum_{M'=-\infty}^{+\infty}J^2_{|M'|}(|q_xR_0|)[N_0\delta(E_{k_\parallel}-E_{|\mathbf{k}_\parallel-\mathbf{q}_\parallel|}-M'\hbar\Omega_{\mathrm{L}}-\hbar\omega_{\mathrm{LO}}$$
$$+\hbar\Omega^z_{nn'})f_{n'}(E^z_{n'}+E_{k_\parallel}-M'\hbar\Omega_{\mathrm{L}}-\hbar\omega_{\mathrm{LO}}+\hbar\Omega^z_{nn'},t)+(N_0+1)\delta(E_{k_\parallel}-E_{|\mathbf{k}_\parallel+\mathbf{q}_\parallel|}-M'\hbar\Omega_{\mathrm{L}}+\hbar\omega_{\mathrm{LO}}$$
$$+\hbar\Omega^z_{nn'})f_{n'}(E^z_{n'}+E_{k_\parallel}-M'\hbar\Omega_{\mathrm{L}}+\hbar\omega_{\mathrm{LO}}+\hbar\Omega^z_{nn'},t)]-\frac{2\pi\alpha}{\hbar\mathcal{S}}f_n(E^z_n+E_{k_\parallel},t)\sum_{n',\mathbf{q}_\parallel}\mathcal{F}_{nn'}(q_\parallel)$$
$$\times\sum_{M'=-\infty}^{+\infty}J^2_{|M'|}(|q_xR_0|)\{N_0\delta(E_{k_\parallel}-E_{|\mathbf{k}_\parallel+\mathbf{q}_\parallel|}-M'\hbar\Omega_{\mathrm{L}}+\hbar\omega_{\mathrm{LO}}+\hbar\Omega^z_{nn'})$$
$$\times[1-f_{n'}(E^z_{n'}+E_{k_\parallel}-M'\hbar\Omega_{\mathrm{L}}+\hbar\omega_{\mathrm{LO}}+\hbar\Omega^z_{nn'},t)]+(N_0+1)\delta(E_{k_\parallel}-E_{|\mathbf{k}_\parallel-\mathbf{q}_\parallel|}$$
$$-M'\hbar\Omega_{\mathrm{L}}-\hbar\omega_{\mathrm{LO}}+\hbar\Omega^z_{nn'})[1-f_{n'}(E^z_{n'}+E_{k_\parallel}-M'\hbar\Omega_{\mathrm{L}}-\hbar\omega_{\mathrm{LO}}+\hbar\Omega^z_{nn'},t)]\}. \quad (6)$$

For $f_n(E_n^z+E_{k_\parallel},t)$, the energy $E_{k_\parallel}$ is measured from the subband edge E_n^z and $\hbar\Omega^z_{nn'}=E^z_n-E^z_{n'}$. Here, the optical phonons are assumed to be in equilibrium for simplicity,[17] and their distribution is given by the Bose distribution $N_0=1/[\exp(\hbar\omega_{\mathrm{LO}}/k_{\mathrm{B}}T)-1]$. The use of nonequilibrium phonon distribution by solving another Boltzmann equation for phonons will slightly change the magnitude of phonon-scattering rates, but the unique features predicted in this paper remain unchanged. It is important to note that photon-assisted intersubband optical-phonon-scattering is different from direct field-induced intersubband electron transitions.[18]

Using the calculated results listed in the Appendix we rewrite Eq. (6) to leading order $O(q_\parallel^2)$ as

$$\frac{\partial}{\partial t}f_n(E_n^z+E_{k_\parallel},t)=[1-f_n(E_n^z+E_{k_\parallel},t)]\sum_{n'}\{[N_0\mathcal{B}^{(1)}_{n,n';-1}(E_{k_\parallel})f_{n'}(E^z_{n'}+E_{k_\parallel}+\hbar\Omega_{\mathrm{L}}-\hbar\omega_{\mathrm{LO}}+\hbar\Omega^z_{nn'},t)+(N_0+1)$$
$$\times\mathcal{B}^{(2)}_{n,n';-1}(E_{k_\parallel})f_{n'}(E^z_{n'}+E_{k_\parallel}+\hbar\Omega_{\mathrm{L}}+\hbar\omega_{\mathrm{LO}}+\hbar\Omega^z_{nn'},t)]+[N_0\mathcal{A}^{(1)}_{n,n';0}(E_{k_\parallel})f_{n'}(E^z_{n'}+E_{k_\parallel}-\hbar\omega_{\mathrm{LO}}+\hbar\Omega^z_{nn'},t)$$
$$+(N_0+1)\mathcal{A}^{(2)}_{n,n';0}(E_{k_\parallel})f_{n'}(E^z_{n'}+E_{k_\parallel}+\hbar\omega_{\mathrm{LO}}+\hbar\Omega^z_{nn'},t)]+[N_0\mathcal{B}^{(1)}_{n,n';1}(E_{k_\parallel})f_{n'}(E^z_{n'}+E_{k_\parallel}-\hbar\Omega_{\mathrm{L}}$$
$$-\hbar\omega_{\mathrm{LO}}+\hbar\Omega^z_{nn'},t)+(N_0+1)\mathcal{B}^{(2)}_{n,n';1}(E_{k_\parallel})f_{n'}(E^z_{n'}+E_{k_\parallel}-\hbar\Omega_{\mathrm{L}}+\hbar\omega_{\mathrm{LO}}+\hbar\Omega^z_{nn'},t)]\}-f_n(E^z_n+E_{k_\parallel},t)$$
$$\times\sum_{n'}\{N_0\mathcal{B}^{(2)}_{n,n';-1}(E_{k_\parallel})[1-f_{n'}(E^z_{n'}+E_{k_\parallel}+\hbar\Omega_{\mathrm{L}}+\hbar\omega_{\mathrm{LO}}+\hbar\Omega^z_{nn'},t)]+(N_0+1)\mathcal{B}^{(1)}_{n,n';-1}(E_{k_\parallel})$$
$$\times[1-f_{n'}(E^z_{n'}+E_{k_\parallel}+\hbar\Omega_{\mathrm{L}}-\hbar\omega_{\mathrm{LO}}+\hbar\Omega^z_{nn'},t)]+N_0\mathcal{A}^{(2)}_{n,n';0}(E_{k_\parallel})[1-f_{n'}(E^z_{n'}+E_{k_\parallel}+\hbar\omega_{\mathrm{LO}}$$
$$+\hbar\Omega^z_{nn'},t)]+(N_0+1)\mathcal{A}^{(1)}_{n,n';0}(E_{k_\parallel})[1-f_{n'}(E^z_{n'}+E_{k_\parallel}-\hbar\omega_{\mathrm{LO}}+\hbar\Omega^z_{nn'},t)]+N_0\mathcal{B}^{(2)}_{n,n';1}(E_{k_\parallel})$$
$$\times[1-f_{n'}(E^z_{n'}+E_{k_\parallel}-\hbar\Omega_{\mathrm{L}}+\hbar\omega_{\mathrm{LO}}+\hbar\Omega^z_{nn'},t)]+(N_0+1)\mathcal{B}^{(1)}_{n,n';1}(E_{k_\parallel})$$
$$\times[1-f_{n'}(E^z_{n'}+E_{k_\parallel}-\hbar\Omega_{\mathrm{L}}-\hbar\omega_{\mathrm{LO}}+\hbar\Omega^z_{nn'},t)]\}. \quad (7)$$

Here, the terms proportional to $-f_n(E_n^z+E_{k_\parallel},t)$ at the end represent electrons scattered out of the state considered, while the terms proportional to $[1-f_n(E_n^z+E_{k_\parallel},t)]$ represent electrons scattered into that state. In Eq. (7), $\mathcal{A}^{(1)}_{n,n';0}(E_{k_\parallel})$ and $\mathcal{A}^{(2)}_{n,n';0}(E_{k_\parallel})$ for the scattering-in case are the rates of phonon absorption and emission in the absence of the laser field, while $\mathcal{B}^{(1)}_{n,n';\pm1}(E_{k_\parallel})$ and $\mathcal{B}^{(2)}_{n,n';\pm1}(E_{k_\parallel})$ are the rates of induced phonon absorption and emission in the presence of the laser field. For the scattering-out case, however, the roles played by $\mathcal{A}^{(1)}_{n,n';0}(E_{k_\parallel})$ and $\mathcal{A}^{(2)}_{n,n';0}(E_{k_\parallel})$, as well as the roles played by $\mathcal{B}^{(1)}_{n,n';\pm1}(E_{k_\parallel})$ and $\mathcal{B}^{(2)}_{n,n';\pm1}(E_{k_\parallel})$, are reversed. It is clear from Eq. (7) that all the intrasubband and intersubband electron transitions associated with the phonon and photon absorption or emission are allowed. However, the extremely small population of electrons at very high energies

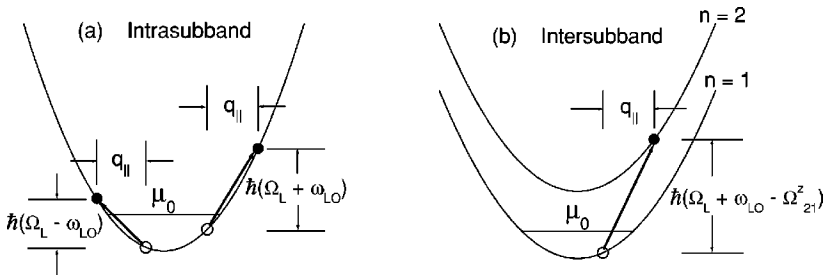

FIG. 1. (a) Illustration of photon-absorption-induced phonon scattering by intrasubband transitions of electrons and (b) photon-absorption-induced intersubband phonon-scattering of electrons, where $n=1$ and 2 are the indices of the two lowest subbands in a quantum well, μ_0 is the chemical potential of electrons in the quantum well, $q_\parallel$ is the wave number of phonons, and Ω_L and ω_{LO} are the photon and optical-phonon frequencies, respectively.

within the first and second subbands and the strong energy dependence in transition rates $\mathcal{B}^{(1)}_{n,n';\pm1}(E_{k_\parallel})$ and $\mathcal{B}^{(2)}_{n,n';\pm1}(E_{k_\parallel})$ only allow a few of them to be observable. For $n=n'$, the dominant photon-absorption-induced phonon scattering by intrasubband electron transitions is sketched in Fig. 1(a) with phonon absorption (term containing N_0) or emission [term containing (N_0+1)]. For $n\neq n'$, the photon-absorption-induced intersubband phonon-scattering process is sketched in Fig. 1(b) with phonon absorption (term containing N_0). We find the distribution $f_n(E^z_n+x,t)$ to be zero for $x<0$ due to the existence of a gap. Moreover, the initial condition for Eq. (7) is set to be $f_n(E^z_n+x,0)=1/[\exp([E^z_n+x-\mu_0(T)]/k_BT)+1]$, with temperature T and electron chemical potential $\mu_0(T)$ determined by the ionized doped electron density n_{2D}.

III. NUMERICAL RESULTS AND DISCUSSIONS

In this section, we present some numerical results for the induced optical-phonon-scattering of electrons in quantum wells by including the photon-assisted phonon-scattering process in Eq. (7). The pulsed laser is chosen to have a Gaussian profile in time with a pulse-duration time of 1 ps. For the resonant excitation, we take $\hbar\Omega_L+\hbar\omega_{LO}-\hbar\Omega^z_{21}=0$. For the off-resonant excitation, we choose the off-resonant energy $\hbar\Omega_L+\hbar\omega_{LO}-\hbar\Omega^z_{21}>0$. The parameters of two samples chosen for calculations are listed in Tables I and II. The other parameters for the calculations will be given in the figure captions.

Figure 2 shows the difference between the electron distributions of sample 1 with/without the photon-assisted process for nonresonant excitations at the moment of peak pulse $t=t_p$ and $\mathcal{E}_0=350$ kV/cm, $\hbar\Omega_L=56.5$ meV, $T=200$ K, and $\hbar\Omega^z_{21}=82.7$ meV. For the second subband $(n=2)$, the change of electron distribution (dashed curve) exhibits two upward steps at $E_{k_\parallel}=\hbar\Omega_L+\hbar\omega_{LO}-\hbar\Omega^z_{21}=10.1$ meV and $E_{k_\parallel}=\hbar\Omega_L-\hbar\omega_{LO}=20.2$ meV. The higher-energy step (upward arrow) reflects the strong photon-absorption-induced phonon emission by intrasubband transitions of electrons within the second subband, while the lower-energy step (downward arrow) indicates the effect of the photon-absorption-induced phonon absorption by intersubband transitions of electrons from the first to the second subband. For the first subband $(n=1)$, from the difference between the electron distributions with/without photon assistance (solid curve), we find only one upward step at $E_{k_\parallel}=\hbar\Omega_L-\hbar\omega_{LO}$. This higher-energy step also comes from the strong photon-absorption-induced phonon emission by intrasubband transitions of electrons within the first subband.

Figure 3 displays the evolution of the electron distributions $f_1(E^z_1+E_{k_\parallel},t)$ and $f_2(E^z_2+E_{k_\parallel},t)$ of sample 1 for three different times at $\mathcal{E}_0=350$ kV/cm, $\hbar\Omega_L=56.5$ meV, $T=200$ K, and $\hbar\Omega^z_{21}=82.7$ meV. From Fig. 3(a), we find that the weak early-time upward step for $E_{k_\parallel}=\hbar\Omega_L-\hbar\omega_{LO}$ at $(t-t_p)/t_p=-0.5$ (dashed curve) is gradually enhanced with time (see solid and dash-dotted curves). This step reflects the enhanced populations of electrons in higher-energy states due to emitting phonons and absorbing photons simultaneously by electrons at the first-subband edge. As shown in Fig. 3(b), we find that the features associated with the two upward steps become much more clear, although $f_2(E^z_2+E_{k_\parallel},t)$ in Fig. 3(b) is one order of magnitude less than $f_1(E^z_1+E_{k_\parallel},t)$ in Fig. 3(a). Both steps (upward and down-

TABLE I. Parameters of GaAs/Al_xGa_{1-x}As single-quantum-well samples chosen for numerical calculations with well width L_W, electron density n_{2D}, well depth V_0, relative dielectric constants $\epsilon_r(\infty)$ and $\epsilon_r(0)$, optical-phonon energy $\hbar\omega_{LO}$, and electron effective mass m^* with m_e being the free-electron mass.

Sample	L_W (Å)	n_{2D} (10^{11} cm^{-2})	V_0 (meV)	$\epsilon_r(\infty)$	$\epsilon_r(0)$	$\hbar\omega_{LO}$ (meV)	m^* (m_e)
1	105	5.25	246	13.2	10.9	36.3	0.067
2	90	5.25	246	13.2	10.9	36.3	0.067

TABLE II. Calculated parameters of GaAs/Al_xGa_{1-x}As single-quantum-well samples chosen for numerical calculations with ground-state energy E^z_1, first-excited-state energy E^z_2, and chemical potential μ_0 at 200 K.

Sample	E^z_1 (meV)	E^z_2 (meV)	$\hbar\Omega^z_{21}$ (meV)	$\mu_0-E^z_1$ (meV)
1	28.1	110.8	82.7	11.52
2	35.1	137.2	102.1	11.52

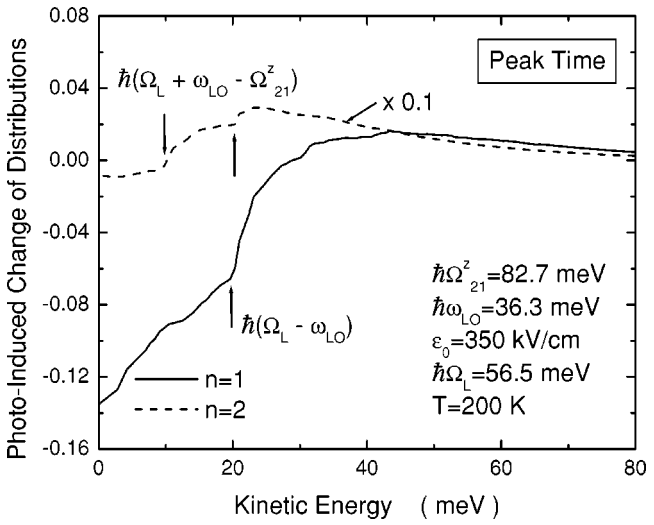

FIG. 2. Difference between the electron distributions of sample 1 with/without the photon-assisted process at $t=t_p$, with t_p being the time at which the pulse peak is reached for the first subband $f_1(E_1^z+E_{k_\parallel},t)$ (solid curve) and the second subband $f_2(E_2^z+E_{k_\parallel},t)$ (dashed curve), with $\mathcal{E}_0=350$ kV/cm, $\hbar\Omega_L=56.5$ meV, $T=200$ K, and $\hbar\Omega_{21}^z=82.7$ meV. The labels, as well as the downward and upward arrows, in the figure indicate different energy positions of upward steps. The dashed curve is amplified by one order of magnitude.

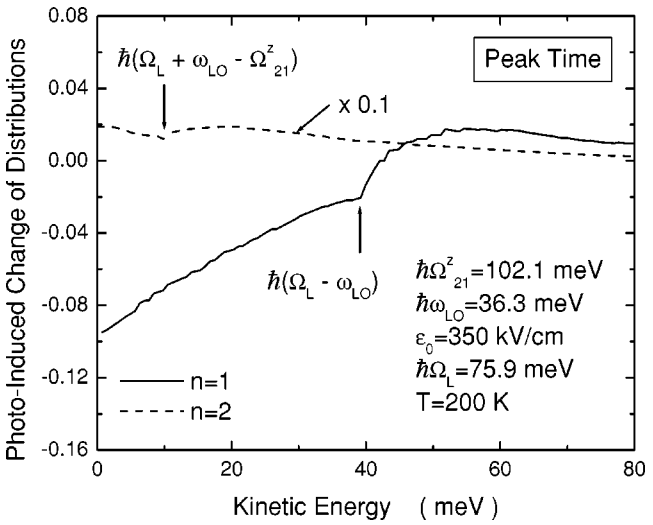

FIG. 4. Difference between the electron distributions of sample 2 with/without the photon-assisted process at $t=t_p$ for $f_1(E_1^z+E_{k_\parallel},t)$ (solid curve) and $f_2(E_2^z+E_{k_\parallel},t)$ (dashed curve), with $\mathcal{E}_0=350$ kV/cm, $\hbar\Omega_L=75.9$ meV, $T=200$ K, and $\hbar\Omega_{21}^z=102.1$ meV. The labels, as well as the downward and upward arrows, in the figure indicate different energy positions of upward steps. The dashed curve is amplified by one order of magnitude.

ward arrows) enhance with time. This is attributed to the fact that electrons are moved from the second-subband edge to higher-energy states due to photon-absorption-induced phonon emission (upward arrow) via intrasubband transition of electrons, as well as from the first subband to the second subband due to photon-absorption-induced phonon absorption.

Figure 4 presents the difference between the electron distributions of sample 2 with/without the photon-assisted process at $t=t_p$ and $\mathcal{E}_0=350$ kV/cm, $\hbar\Omega_L=75.9$ meV, $T=200$ K, and $\hbar\Omega_{21}^z=102.1$ meV. Here, the increase of the photon energy $\hbar\Omega_L$ for the same off-resonant energy due to reduced well width greatly reduces the effect of photon-absorption-induced phonon-scattering of electrons for the same value of $\mathcal{E}_0$ because of reduced R_0. Compared with Fig. 2 for $n=1$ (solid curve), the upward step (upward arrow) at $E_{k_\parallel}=\hbar\Omega_L-\hbar\omega_{LO}$ is shifted from 20.2 meV to a higher energy of 39.6 meV, as expected. For $n=2$ (dashed curve), only one lower-energy upward step (downward arrow) at $E_{k_\parallel}=\hbar\Omega_L+\hbar\omega_{LO}-\hbar\Omega_{21}^z=10.1$ meV is clearly visible.

Figure 5 exhibits the difference between the electron distribution of sample 1 with/without the photon-assisted process at $t=t_p$ and $\mathcal{E}_0=350$ kV/cm, $\hbar\Omega_L=56.5$ meV, $T=150$ K, and $\hbar\Omega_{21}^z=82.7$ meV. Compared with Fig. 2, the photon-absorption-induced phonon absorption by intersubband transitions of electrons from the first to the second subband (downward arrow) at $T=150$ K is reduced, as is the photon-absorption-induced phonon emission within the second subband (upward arrow) for $n=2$ (dashed curve). However, for the case with $n=1$ (solid curve), we find only insignificant change compared with the solid curve in Fig. 2.

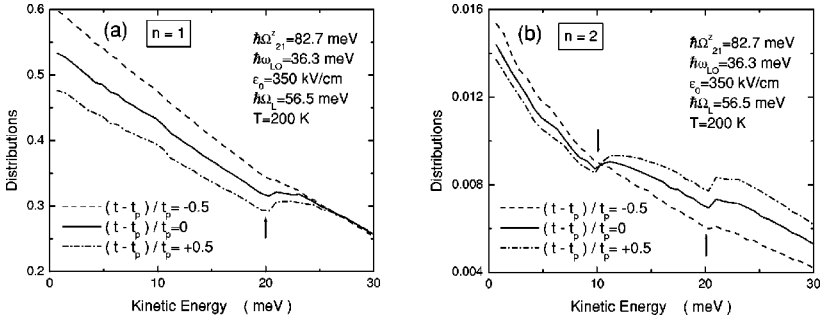

FIG. 3. Electron distributions of sample 1 with the photon-assisted process for (a) the first subband and the second subband at three different times, with $\mathcal{E}_0=350$ kV/cm, $\hbar\Omega_L=56.5$ meV, $T=200$ K, and $\hbar\Omega_{21}^z=82.7$ meV. The downward and upward arrows in the figures indicate different energy positions of upward steps seen in Fig. 2. The dashed, solid and dash-dotted curves are for $(t-t_p)/t_p=-0.5$, 0, and 0.5, respectively.

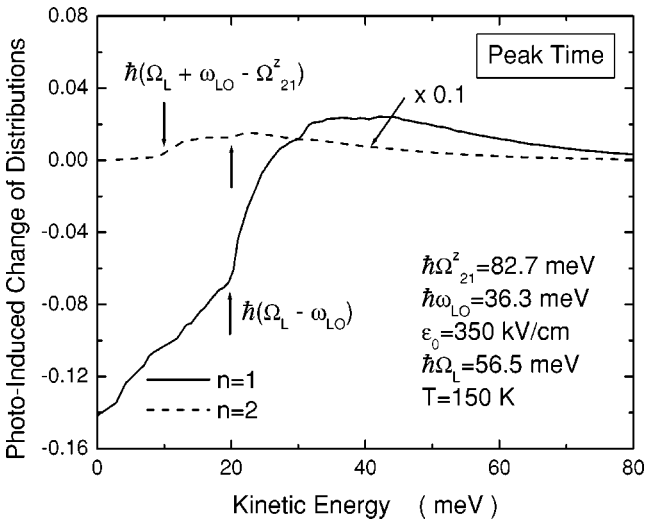

FIG. 5. Difference between the electron distributions of sample 1 with/without the photon-assisted process at $t=t_p$ for $f_1(E_1^z+E_{k_\parallel},t)$ (solid curve) and $f_2(E_2^z+E_{k_\parallel},t)$ (dashed curve), with $\mathcal{E}_0=350$ kV/cm, $\hbar\Omega_L=56.5$ meV, $T=150$ K, and $\hbar\Omega_{21}^z=82.7$ meV. The labels, as well as the downward and upward arrows, in the figure indicate different energy positions of upward steps. The dashed curve is amplified by one order of magnitude.

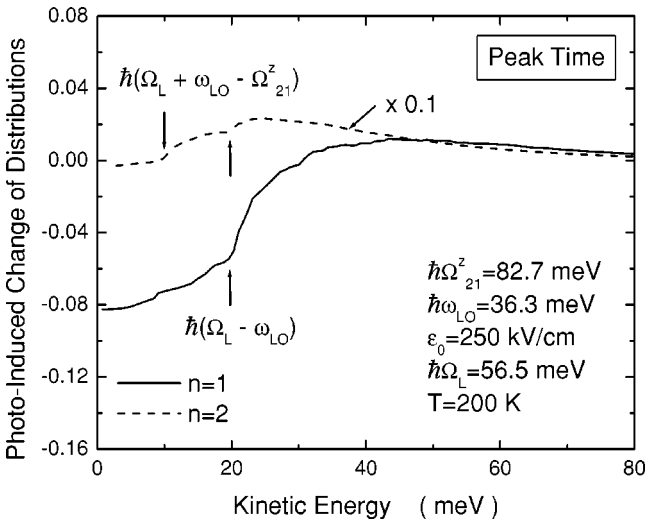

FIG. 6. Difference between the electron distributions of sample 1 with/without the photon-assisted process at $t=t_p$ for $f_1(E_1^z+E_{k_\parallel},t)$ (solid curve) and $f_2(E_2^z+E_{k_\parallel},t)$ (dashed curve), with $\mathcal{E}_0=250$ kV/cm, $\hbar\Omega_L=56.5$ meV, $T=200$ K, and $\hbar\Omega_{21}^z=82.7$ meV. The labels, as well as the downward and upward arrows, in the figure indicate different energy positions of upward steps. The dashed curve is amplified by one order of magnitude.

We display in Fig. 6 the difference between the electron distributions of sample 1 with/without the photon-assisted process at $t=t_p$ and $\mathcal{E}_0=250$ kV/cm, $\hbar\Omega_L=56.5$ meV, $T=200$ K, and $\hbar\Omega_{21}^z=82.7$ meV. Compared with Fig. 2, the decrease in $\mathcal{E}_0$ only slightly reduces the effects of photon-absorption-induced phonon emission and absorption. Since $R_0\propto\mathcal{E}_0/\Omega_L^2$, we expect a smaller reduction in photon-assisted effects when $\mathcal{E}_0$ decreases in Fig. 6 in comparison to the case when $\hbar\Omega_L$ increases in Fig. 4 for the same off-resonant energy.

We present in Fig. 7 the difference between the electron distributions of sample 1 with/without the photon-assisted process at $t=t_p$ and $\mathcal{E}_0=350$ kV/cm, $\hbar\Omega_L=66.5$ meV, $T=200$ K, and $\hbar\Omega_{21}^z=82.7$ meV. Compared with Fig. 2, the increase of photon energy $\hbar\Omega_L$ (different off-resonant energy) in this case first weakens the effect of photon-absorption-induced phonon emission and absorption. The increase of $\hbar\Omega_L$ pushes all the steps (downward and upward arrows) to higher energies. Therefore, the reduction of coefficients $\mathcal{B}^{(1)}_{n,n';\pm1}(E_{k_\parallel})$ and $\mathcal{B}^{(2)}_{n,n';\pm1}(E_{k_\parallel})$ with $E_{k_\parallel}$ further weakens the step features in Fig. 7.

IV. CONCLUSIONS AND REMARKS

In the presence of a normally incident mid-IR pulsed laser field, we have found a unique photon-absorption-induced intersubband optical-phonon-scattering of electrons from the first to the second subband in quantum wells by including the photon-assisted phonon-scattering process in a Boltzmann equation beyond the relaxation-time approximation. We have seen that a renormalized electron-phonon interaction arises from the presence of the laser field. The laser field increases the electron kinetic energy, and the increased electron energy can be exchanged with phonons or used to promote the electrons to higher subbands. These processes significantly change the population of electrons in both subbands. We have also studied the difference between the electron distributions with/without the photon-assisted process for two subbands with various lattice temperatures, photon energies, laser-field strengths, and quantum-well widths. We have found upward steps in the difference between the electron

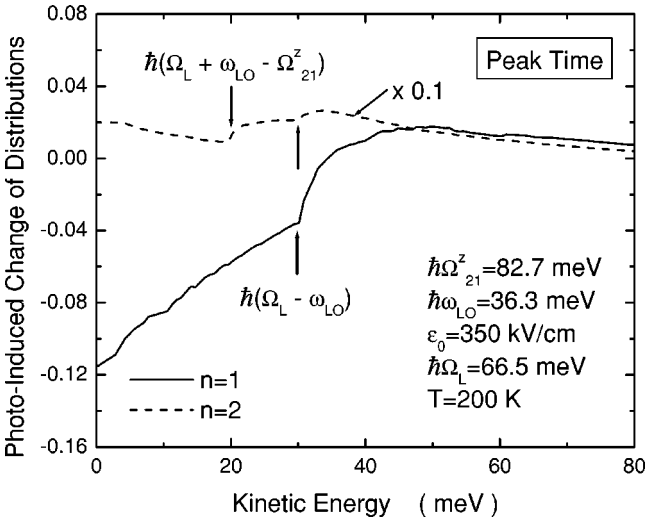

FIG. 7. Difference between the electron distributions of sample 1 with/without the photon-assisted process at $t=t_p$ for $f_1(E_1^z+E_{k_\parallel},t)$ (solid curve) and $f_2(E_2^z+E_{k_\parallel},t)$ (dashed curve), with $\mathcal{E}_0=350$ kV/cm, $\hbar\Omega_L=66.5$ meV, $T=200$ K, and $\hbar\Omega_{21}^z=82.7$ meV. The labels, as well as the downward and upward arrows, in the figure indicate different energy positions of upward steps. The dashed curve is amplified by one order of magnitude.

distributions with/without the photon-assisted process and attributed them to either the photon-absorption-induced phonon-scattering by intrasubband transitions of electrons or the photon-absorption-induced intersubband phonon-scattering process of electrons. The main features revealed in this study include the occurrence of a forbidden photon absorption for a plane-polarized laser field with $\hbar\Omega_{\rm L} \ll \hbar\Omega_{21}^{z}$, as well as the occurrence of ''forbidden'' intersubband phonon-scattering of electrons for phonon energy $\hbar\omega_{\rm LO} \ll \hbar\Omega_{21}^{z}$. The features presented in this paper are not limited to the samples used in the calculations. The calculated hot-electron distribution can be used to evaluate the nonequilibrium electron temperature and the average electron energy, which play crucial roles in understanding laser damage of semiconductor materials.[2,9]

Phonon scattering is a first-order contribution, while the Coulomb scattering is a second-order contribution. Neglecting the Coulomb scattering in comparison with phonon-scattering requires

$$n_{\rm 2D} < \frac{4m^*\epsilon_{\rm r}(0)\hbar\omega_{\rm LO}}{\pi\hbar^2}\left[\frac{1}{\epsilon_{\rm r}(\infty)} - \frac{1}{\epsilon_{\rm r}(0)}\right].$$

Moreover, the first-order Coulomb effect is the Hartree-Fock correction. Neglecting the Hartree-Fock correction to the electron energy requires

$$n_{\rm 2D} > \frac{1}{\pi a_{\rm B}^2}\left(\frac{4a_{\rm B}}{3L_{\rm W}}\right)^{1/2},$$

where $a_{\rm B} = 4\pi\epsilon_0\epsilon_{\rm r}(0)\hbar^2/m^*e^2$ is the Bohr radius of electrons in GaAs well material. For samples 1 and 2, the electron densities used in the calculations [see Tables I and II] satisfy these two requirements. This justifies neglecting both the Hartree-Fock correction to electron energy and the Coulomb scattering as a contribution to the collision integral.

The spatially uniform field only couples to the center-of-mass motion of electron gases, and the center-of-mass moves with a drift velocity in space. The dynamics for scattering of electrons, including electron-impurity, electron-phonon, and electron-electron scattering, is seen only in the relative motion of electrons. The drift of electrons due to a dc electric field gives rise to a Doppler shift in the scattering of electrons with static lattice or impurity atoms. The drift of electrons due to an electromagnetic field, on the other hand, gives rise to a renormalization of electron scattering with static lattice or impurity atoms.[8,19] In this paper, only the drift of electrons due to an electromagnetic field exists, which has been included in the Bessel function in Eq. (6).

ACKNOWLEDGMENTS

One of the authors (T.A.) was supported by the National Research Council. We wish to thank P. M. Alsing for numerous very helpful discussions on the subject. We would also like to thank AHPCC where some of these calculations were carried out.

APPENDIX

Here, we calculate the coefficients $\mathcal{A}^{(1,2)}_{n,n';0}(E_{k_\parallel})$ and $\mathcal{B}^{(1,2)}_{n,n';\pm1}(E_{k_\parallel})$ introduced in Eq. (7). For a weak incident laser field, q_xR_0 is small. As a result, we retain only $J_0(|q_xR_0|)$ and $J_1(|q_xR_0|)$ by setting $M' = 0, \pm 1$ in the Boltzmann equation (6), which leads to Eq. (7). Finally, we obtain

$$\mathcal{A}^{(1)}_{n,n';0}(E_{k_\parallel}) = \frac{2\pi\alpha}{\hbar\mathcal{S}}\sum_{\mathbf{q}_\parallel}\mathcal{F}_{nn'}(q_\parallel)\langle\langle J_0^2(|q_xR_0|)\rangle\rangle\,\delta^{(1)}_{n,n';0}, \tag{A1}$$

$$\mathcal{A}^{(2)}_{n,n';0}(E_{k_\parallel}) = \frac{2\pi\alpha}{\hbar\mathcal{S}}\sum_{\mathbf{q}_\parallel}\mathcal{F}_{nn'}(q_\parallel)\langle\langle J_0^2(|q_xR_0|)\rangle\rangle\,\delta^{(2)}_{n,n';0}, \tag{A2}$$

$$\mathcal{B}^{(1)}_{n,n';\pm1}(E_{k_\parallel}) = \frac{2\pi\alpha}{\hbar\mathcal{S}}\sum_{\mathbf{q}_\parallel}\mathcal{F}_{nn'}(q_\parallel)\langle\langle J_1^2(|q_xR_0|)\rangle\rangle\,\delta^{(1)}_{n,n';\pm1}, \tag{A3}$$

$$\mathcal{B}^{(2)}_{n,n';\pm1}(E_{k_\parallel}) = \frac{2\pi\alpha}{\hbar\mathcal{S}}\sum_{\mathbf{q}_\parallel}\mathcal{F}_{nn'}(q_\parallel)\langle\langle J_1^2(|q_xR_0|)\rangle\rangle\,\delta^{(2)}_{n,n';\pm1}. \tag{A4}$$

In Eqs. (A1)–(A4), we have defined for $M = \pm 1$,

$$\begin{bmatrix}\delta^{(1)}_{n,n';M}\\ \delta^{(2)}_{n,n';M}\end{bmatrix} = \begin{bmatrix}\delta(E_{k_\parallel} - E_{|\mathbf{k}_\parallel - \mathbf{q}_\parallel|} - M\hbar\Omega_{\rm L} - \hbar\omega_{\rm LO} + \hbar\Omega^{z}_{nn'})\\ \delta(E_{k_\parallel} - E_{|\mathbf{k}_\parallel + \mathbf{q}_\parallel|} - M\hbar\Omega_{\rm L} + \hbar\omega_{\rm LO} + \hbar\Omega^{z}_{nn'})\end{bmatrix}. \tag{A5}$$

[1] T. Ando, A.B. Fowler, and F. Stern, Rev. Mod. Phys. **54**, 437 (1982).
[2] A. Kaiser, B. Rethfeld, H. Vicanek, and G. Simon, Phys. Rev. B **61**, 11 437 (2000).
[3] N.W. Ashcroft and N.D. Mermin, *Solid State Physics* (Saunders, Philadephia, 1976), Chaps. 8–11.
[4] C.S. Ting, S.C. Ying, and J.J. Quinn, Phys. Rev. B **14**, 4439 (1976).
[5] X.L. Lei and C.S. Ting, Phys. Rev. B **32**, 1112 (1985).
[6] W. Xu and C. Zhang, Phys. Rev. B **55**, 5259 (1997).
[7] M. Lindberg and S.W. Koch, Phys. Rev. B **38**, 3342 (1988).
[8] X.L. Lei, J. Appl. Phys. **84**, 1396 (1998).
[9] T. Apostolova, D.H. Huang, P.M. Alsing, J. McIver, and D.A. Cardimona, Phys. Rev. B **66**, 075208 (2002).
[10] S.K. Lyo, Phys. Rev. B **43**, 2412 (1991).
[11] L. Besombes, K. Kheng, L. Marsal, and H. Mariette, Phys. Rev. B

63, 155307 (2001).
[12] J.N. Fehr, M.A. Dupertuis, T.P. Hessler, L. Kappei, D. Marti, F. Salleras, M.S. Nomura, B. Deveaud, J.Y. Emery, and B. Dagens, IEEE J. Quantum Electron. **QE-38**, 674 (2002).
[13] B.Y.-K. Hu and S. Das Sarma, Phys. Rev. B **44**, 8319 (1991).
[14] M. Sparks, D.L. Mills, R. Warren, T. Holstein, A.A. Maradudin, L.J. Sham, E. Loh, Jr., and D.F. King, Phys. Rev. B **24**, 3519 (1981).
[15] X.-G. Zhao, G.A. Georgakis, and Q. Niu, Phys. Rev. B **56**, 3976 (1997).
[16] W. Li and L.E. Reichl, Phys. Rev. B **60**, 15 732 (1999).
[17] W. Yu, Physica E (Amsterdam) **11**, 257 (2001).
[18] D.H. Huang and M.O. Manasreh, Phys. Rev. B **54**, 5620 (1996).
[19] M.I. Stockman, L.N. Pandey, and T.F. George, Phys. Rev. Lett. **65**, 3433 (1990).